ALD-based Confined PCM with a Metallic Liner toward Unlimited Endurance

W. Kim[1], M. BrightSky[1], T. Masuda[2], N. Sosa[1], S. Kim[1], R. Bruce[1], F. Carta[1], G. Fraczak[1], H. Y. Cheng[3], A. Ray[1], Y. Zhu[1], H. L. Lung[3], K. Suu[2] and C. Lam[1]

[1]IBM T. J. Watson Research Center, Yorktown Heights, NY, USA, email: wkim@us.ibm.com

[2]ULVAC, Inc., Shizuoka, Japan, [3]Macronix International Co., Ltd., Emerging Central Lab., Hsinchu, Taiwan, ROC

***Abstract*—** We present for the first time in-depth analysis of the outstanding endurance characteristics of an ALD-based confined phase change memory (PCM) [1] with a thin metallic liner. Experimental results confirm that both the proper metallic liner and the confined pore cell structure are required for a reliability advantage. This confined PCM with a metallic liner is found to be immune to classic endurance failure mechanisms. The void-free confined PCM yields a new record endurance ($2x10^{12}$ cycles) with stabilized elemental segregation that does not result in stuck-SET failure.

I. INTRODUCTION

PCM is a prime candidate for storage class memory (SCM) [2]. However, most reported PCM cells show stuck-SET failure caused by elemental segregation [3,4,5] or open failure (void formation) [7] as their failure mechanisms. In order to overcome these well-known failure mechanisms for PCM, we fabricated a novel confined PCM cell with a thin metallic liner as shown in Fig. 1 [1]. In addition to previously reported benefit of metallic liner such as drift and noise mitigation [8, 9], this confined cell structure with ALD GST and a metallic liner brings the programming endurance beyond $2x10^{12}$ cycles. In this paper, we thoroughly investigate the outstanding endurance of the novel confined PCM that is free from the endurance failure mechanisms.

II. EXPERIMENTAL RESULTS

A. The Effect of a Metallic Liner

Fig. 2 shows the distributions of initial resistances with and without liner A. The yield of the PCM cells without liner is not good due to many open bits caused by voids inside the pores (the bits with R_{init} of 1GΩ are open bits in Fig. 2). However, ALD GST inside the pore is found to be void-free and dense with metallic liner A in Fig. 2(b). These experiments indicate that the metallic liner helps ALD GST grow inside pore without voids. So, we explored different metallic liners for the confined PCM and found two great candidates (liner A and liner B) that show low as-fabricated resistance (Fig. 3(c)). This means that both liners result in dense ALD GST without any voids inside the pores. As illustrated in Fig. 3(a), (b), liner A successfully prevented void generation during cycling while liner B did not. It is clear that liner A serves as a better surfactant layer for the confined PCM cell than liner B. Thus, we conclude that liner A is a proper metallic liner that can catalyze ALD GST growth in the pore and help to improve endurance by preventing void formation during programming.

After full integration, typical median R-I curve of the Sb-rich confined PCM array with liner A is shown in Fig. 4(a), with tight distributions of the SET and RESET resistances in Fig. 4(b). The open symbols in Fig. 4(a) represent +/- 30%. 10X switching window is also observed. Low as-fabricated resistance that is comparable to SET resistance suggests that the ALD GST inside the pore is fully crystalline as fabricated without any voids. Next, outstanding endurance results with this fully integrated confined PCM array will be discussed.

B. New Record Endurance with the Confined PCM Cell

The Sb-rich confined PCM with liner A survived $2x10^{12}$ cycles and it is still alive without any voids as shown in Fig. 5. This ALD-based confined PCM finally beats the previous endurance record for PCM which was $1.25x10^{12}$ cycles [10]. Moreover, Fig. 6 shows that even after $7x10^{14}$ RESET-only programming cycles and additional 10^{12} SET-RESET programming cycles, the Sb-rich confined PCM cell is still switching without degradation. This is also a new record of RESET-only endurance for PCM. In Fig. 6(d), another Sb-rich confined PCM cell with liner A also remains dense without any voids after 10^{11} SET-only programming cycles. Almost constant SET resistances over the SET-only programming cycles represents that this confined PCM cell is fully crystalline and therefore no further crystallization is necessary. All these experimental results exhibit the robustness of the Sb-rich confined PCM with liner A that can withstand a lot of electrical and thermal stress during cycling without generating voids.

In addition, a dense, void-free fill is observed on the Te-rich confined PCM with liner A after great endurance beyond $2x10^{11}$ cycles (Fig. 10). After the endurance cycling, 1/3 of the pore near bottom electrode (BE) becomes Sb-rich and 2/3 of the pore near top electrode (TE) becomes Te-rich (Fig. 11). In the confined cell structure, the SET speed of the cell is determined by the GST composition in the switching region of the pore (Fig. 17). As illustrated in Fig. 12, the SET speed of this PCM is much slower (1μs) compared to the Sb-rich confined PCM because of Te-rich GST composition in the active switching region (Fig. 11, Fig. 17). The small confined cell structure with liner A enables excellent endurance regardless of the GST composition inside the pore.

978-1-5090-3902-9/16/$31.00 ©2016 IEEE

IEDM16-83

C. Analysis of the Outstanding Endurance

In order to investigate the outstanding endurance of the confined PCM with a metallic liner, we performed TEM and EDX analysis after various programming cycles. In the first column of Fig. 7, the virgin PCM cell shows uniform GST composition inside the pore. So, in the first programming cycle, the switching region in the pore is located near BE as predicted by COMSOL simulation in Fig. 16(a). The small pore structure and high current density inside the pore enables almost complete elemental segregation during the first few cycles (second column in Fig. 7). As a result, after 10 cycles, 2/3 of the pore near BE already becomes Sb-rich and 1/3 of the pore near TE becomes Te-rich. Especially, GST near BE becomes excessively Sb-rich which is metallic and thermally conductive (Fig. 17). Therefore, this extremely segregated region serves as an extended electrode and switching region (hottest spot) moves up toward the center of the pore (Fig. 15, Fig. 16). In Fig. 7 and Fig. 8, limited numbers of Sb atoms and Te atoms in the small pore prevent significant further segregation during cycling. The segregated elemental distribution is maintained well during cycling without any voids, which gives rise to a consistently fast SET speed (Fig. 9) as well as stable SET and RESET resistances over cycles (Fig. 5, Fig. 6). Thus, the switching region also remains near the center of the pore during entire programming cycles. Moreover, ALD PCM inside the pore is already in an almost equilibrium state where electro-static force nearly matches the diffusion force for both Sb and Te as described in Fig. 16(b). This stabilized elemental segregation explains why the small pore structure with a metallic liner exhibits outstanding endurance.

D. Structural Advantage of the Confined PCM Cell

To investigate the structural advantage of the confined PCM cell, we integrated a PVD-based mushroom PCM that has the same composition as the Sb-rich confined PCM. Based on EDX analysis, the Sb-rich mushroom PCM and the Sb-rich confined PCM are confirmed to be same in the composition within 5%. The heater electrode (BE) in this mushroom PCM cell has identical size as the pore of the confined PCM. Therefore, the mushroom cell requires a lot more RESET current than the confined cell after Sb segregation occurs near BE due to much larger switching volume in the mushroom cell. Moreover, in the mushroom cell, Sb segregation becomes gradually severe over cycles because of much larger amount of Sb outside of the switching region and a lot lower programming current density in the switching region than the pore structure (Fig. 14). So, the switching region still remains near the heater electrode and therefore the SET speed of the mushroom cell is faster (8ns, Fig. 13) than the confined cell (80ns, Fig. 9) since there are more Sb atoms in the switching region [5, 6]. The gradual Sb segregation over cycles makes gradual decrease of both SET and RESET resistances over cycles and finally results in stuck-SET failure which is caused by not enough RESET current (Fig 13. (b)). However, the confined PCM cell can function reliably with consistent programming current without stuck-SET failure. For the confined PCM cell, the diameter of the switching region does not change dramatically during cycling since this pore structure has steep vertical profile with high aspect ratio (~4:1). Thus, the consistent programming current of the confined cell can be explained by the consistent volume of the switching region over cycles. This clearly indicates the strength and robustness of the confined pore structure.

III. CONCLUSION

We have characterized thoroughly our record-breaking endurance ($2x10^{12}$ cycles) of the ALD-based confined PCM with metallic liner A. The small pore structure confines active switching region near the center of the pore during programming (Fig. 15, Fig. 17). In addition, the high programming current density in the small pore results in early elemental segregation inside the pore (Fig. 7, Fig. 8). Because of the stabilized elemental segregation, the extremely segregated regions near both electrodes serve as extended electrodes during programming cycles (Fig. 17). Thus, the confined PCM cell continues to switch (Fig. 5) without stuck-SET failure while the mushroom PCM cell does not (Fig. 13). The proper metallic liner also gives this pore cell structure a reliability benefit by preventing void generation during cycling (Fig. 3 (a)) and mitigating the resistance drift [8]. The Sb-rich confined ALD PCM with liner A is reliable for more than $2x10^{12}$ programming cycles without showing any failure mechanisms and therefore has a high potential to be incorporated into a high density memory-type (M-type) SCM because of its great endurance, fast switching speed, fabrication process free from etching damage, and excellent scalability.

REFERENCES

[1] M. BrightSky et al., "Crystalline-as-Deposited ALD Phase Change Material Confined PCM Cell for High Density Storage Class Memory," *IEDM*, 2015.

[2] C. Lam, "Phase Change Memory and Its intended application," *IEDM*, 2014.

[3] S. Raoux, et al., "Phase change materials and their application to random access memory technology, *Microelectron. Eng.*, vol. 85, no. 12, pp. 2330–2333, 2008.

[4] T.Y. Yang, et al., "Atomic migration in molten and crystalline Ge2Sb2Te5 under high electric field," *Appl. Phys. Lett.* 95, 032104, 2009.

[5] G. Novielli, et al., "Atomic migration in phase change materials," *IEDM*, pp. 22.3.1–22.3.4, 2013.

[6] B. Rajendran, et al., "On the dynamic resistance and reliability of phase change memory," *VLSI Tech. Symp.*, no. 2, pp. 96–97, 2008.

[7] C.F. Chen, et. al., "Endurance Improvement of Ge2Sb2Te5-Based Phase Change Memory," *IMW*, 2009.

[8] S. Kim et al., "A Phase Change Memory Cell with Metallic Surfactant Layer as a Resistance Drift Stabilizer," *IEDM*, 2013.

[9] S. Kim et al., "A Phase Change Memory Cell with Metal Nitride Liner as a Resistance Stabilizer to Reduce Read Current Noise for MLC Optimization," *IEEE TED* (in press).

[10] S. Lai et al., "OUM - A 180 nm Nonvolatile Memory Cell Element Technology For Stand Alone and Embedded Applications," *IEDM*, 2001.

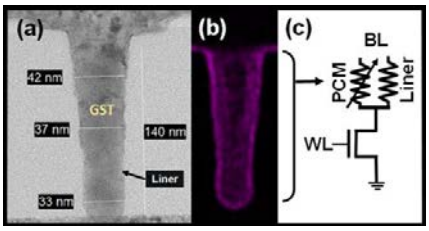

Fig. 1. (a) Sb-rich confined PCM cell with metallic liner A after full integration [1]. (b) Continuous metallic liner A with uniform thickness is confirmed by EDX elemental map. (c) Schematic view of the confined PCM cell with a transistor (1T1R structure).

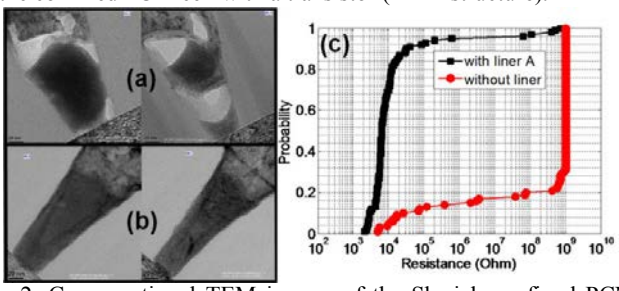

Fig. 2. Cross-sectional TEM images of the Sb-rich confined PCM cells (a) without liner and (b) with liner A after full integration. (c) Probability plot of initial resistances of the Sb-rich confined PCM cells with liner A and without liner.

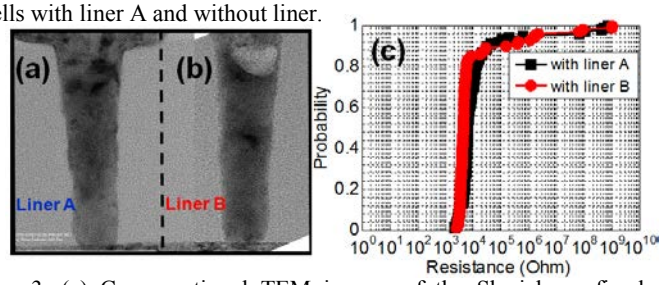

Fig. 3. (a) Cross-sectional TEM images of the Sb-rich confined PCM cells with either (a) liner A or (b) liner B after 10^{11} cycles. (c) Probability plot of initial resistances shows similar low initial resistances with both liner A and liner B.

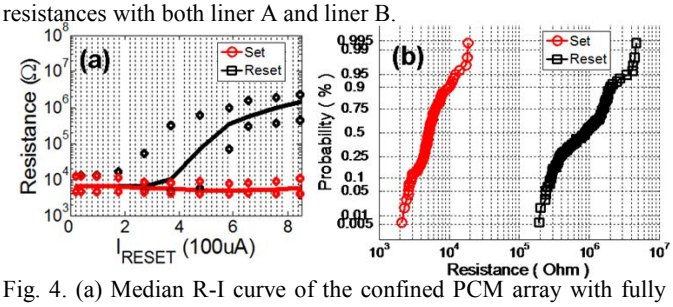

Fig. 4. (a) Median R-I curve of the confined PCM array with fully crystalline Sb-rich ALD GST and metallic liner A. (b) Probability plot of SET and RESET resistances with the confined PCM cells shows tight distribution.

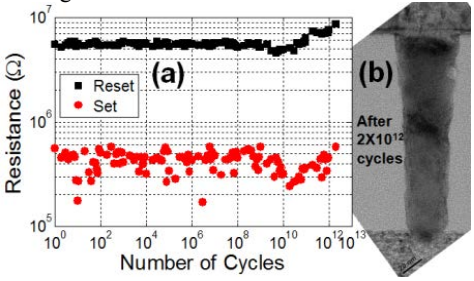

Fig. 5. (a) The Sb-rich confined PCM with liner A exhibits a new endurance record for PCM ($2x10^{12}$ cycles). This cell remains alive.

(b) Cross-sectional TEM image of the cell after $2x10^{12}$ cycles shows dense, void-free PCM inside the pore.

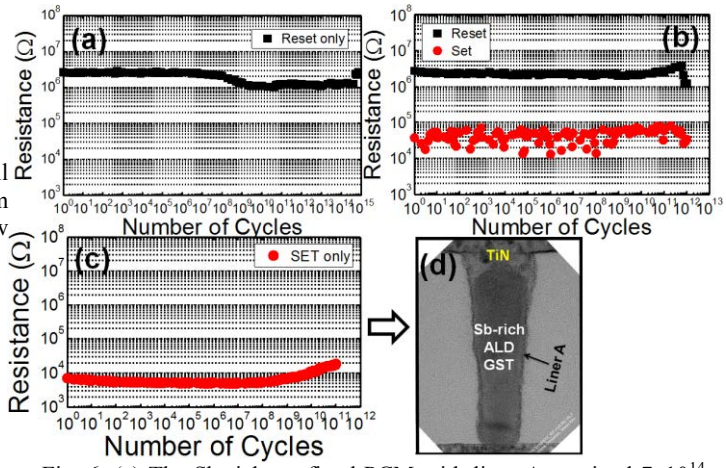

Fig. 6. (a) The Sb-rich confined PCM with liner A survived $7x10^{14}$ cycles of RESET-only programming. (b) After $7x10^{14}$ cycles of RESET-only programming, this Sb-rich confined PCM cell shows outstanding endurance (additional 10^{12} cycles). (c) Another Sb-rich confined PCM cell with liner A went through 10^{11} cycles of SET-only programming without failure. This PCM cell remains dense without any voids in Fig. 6(d).

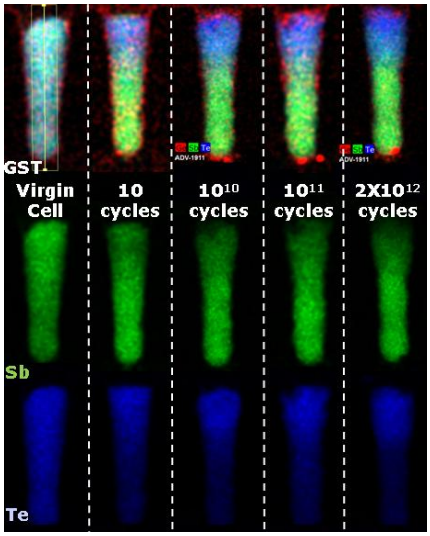

Fig. 7. EDX elemental maps of the Sb-rich confined PCM cells with liner A after different number of programming cycles. Excellent endurance is attributed to stabilized elemental segregation without significant further elemental segregation and generation of voids during cycling.

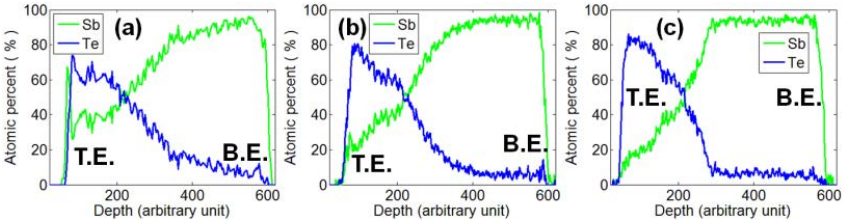

Fig. 8. EDX vertical profiles of the Sb-rich confined PCM cells with liner A after (a) 10 cycles, (b) 10^{10} cycles and (c) $2x10^{12}$ cycles. The early-segregated elemental profile is maintained well during cycling up to $2x10^{12}$ cycles.

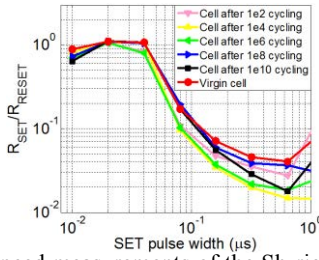

Fig. 9. SET speed measurements of the Sb-rich confined PCM with liner A after various programming cycles. This confined PCM cell shows the consistent SET speed (~80ns) over cycles.

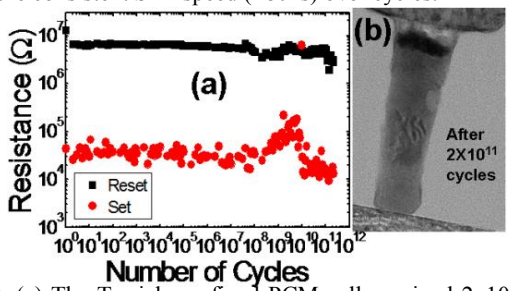

Fig. 10. (a) The Te-rich confined PCM cell survived $2x10^{11}$ cycles with liner A and it is still alive. (b) Cross-sectional TEM image of the confined cell after $2x10^{11}$ cycles shows a dense, void-free fill inside the pore with uniform thickness of liner A.

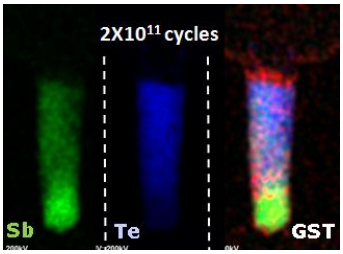

Fig. 11. EDX elemental maps of the Te-rich confined PCM cells with liner A after $2x10^{11}$ cycles.

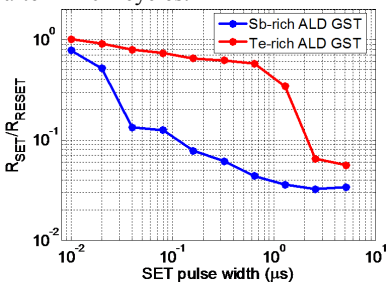

Fig. 12. SET speed comparison between the Sb-rich confined PCM and the Te-rich confined PCM. Both cells have liner A. The Sb-rich confined PCM cell shows much faster SET speed than the Te-rich confined PCM cell.

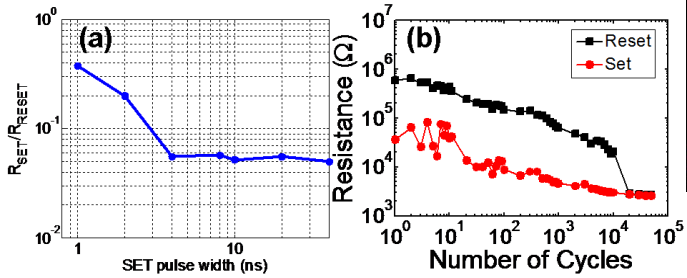

Fig. 13. (a) The SET speed and (b) endurance test result of a PVD-based Sb-rich mushroom PCM cell. The mushroom cell shows super fast SET speed (8ns) and poor endurance (10^4 cycles).

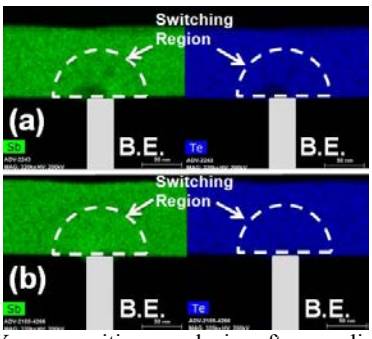

Fig. 14. EDX composition analysis after cycling the Sb-rich mushroom PCM cells. Both cells (a) and (b) end with stuck-SET failure due to gradual elemental segregation. Much lower programming current density in the switching region than the confined cell results in gradual elemental segregation.

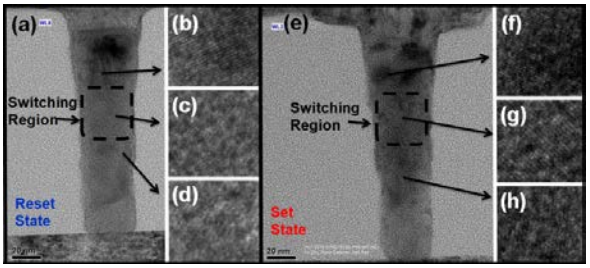

Fig. 15. Cross-sectional TEM images of the Sb-rich confined PCM cells with liner A either (a) in RESET state or (e) in SET state. (a) In RESET state, PCM near (b) TE and (d) BE is crystalline except (c) center region which is amorphous. (e) In SET state, PCM is found to be crystalline inside the entire pore. This confirms that switching occurs near the center of the PCM pore.

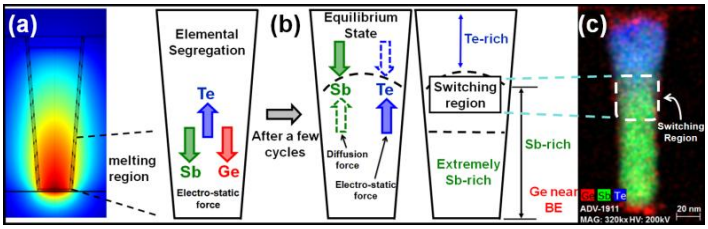

Fig. 16. (a) The COMSOL simulation result and a schematic figure describe the melting region (switching region) and elemental segregation [4] respectively in the confined PCM cell during the first programming. (b), (c) In the following few cycles, the switching region moves up toward the center of the pore (Fig. 15) where electro-static force almost matches diffusion force for both Sb and Te.

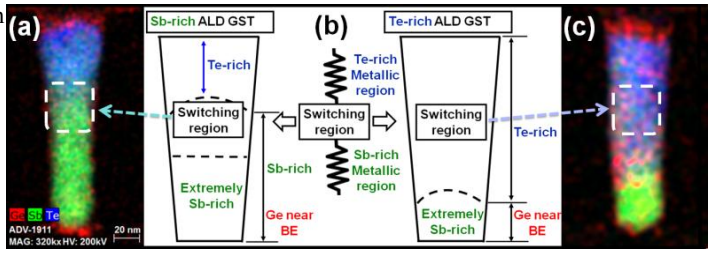

Fig. 17. (b) The schematic figure illustrates switching region and elemental segregation during cycling (a) in the Sb-rich confined PCM cell with liner A and (c) in the Te-rich confined PCM cell with liner A. For both types of cells, the PCM pore is extremely Sb-rich near BE and extremely Te-rich near TE. Each segregated region is metallic and serves as an extended electrode.